FREQUENCY DEPENDENCE OF ELECTRIC CURRENT PERTURBATION PROBE RESPONSE

R. E. Beissner

Southwest Research Institute
6220 Culebra Road
San Antonio, Texas 78284

INTRODUCTION

The electric current perturbation (ECP) probe[1-3] is similar to a conventional eddy current probe in that a coil, typically a cylindrical winding, is used to induce current in the test piece. The ECP probe differs in the use of a separate differential sensor coil, with axis parallel to the surface of the piece, and usually located just outside the induction coil winding. We have found that this sensor orientation tends to minimize probe-to-surface coupling and therefore minimizes liftoff noise.

At our last meeting we reported on development of a computer program that models an ECP probe and it's interaction with a flaw[3]. This program accepts as input the dimensions of induction and sensor coil windings and allows us to predict flaw and liftoff response in a low frequency approximation. This approximation is adequate for many applications of interest because we usually operate at frequencies of the order of 100 kHz or less, and, in low conductivity materials of concern in aircraft engine applications, the skin depth is then much greater than flaw dimensions.

In this article we present an extension of the program to higher frequencies and the introduction of new models of the interaction of current with a flaw and with surface or near surface irregularities in the material. We also describe applications of these new developments to signal/noise calculations for surface flaws as a function of frequency in an attempt to learn more about the optimum operating frequency for the ECP probe.

A FLAW INTERACTION MODEL

Figure 1 illustrates one of the differences between the flaw interaction model used in earlier calculations and the new model used here. The arrows depict incident current density--they are regularly spaced with Model 1 to indicate the assumption of uniform incident current and they vary with position along the flaw length and depth in the new

model, Model 2, to indicate a nonuniform distribution over the crack face.

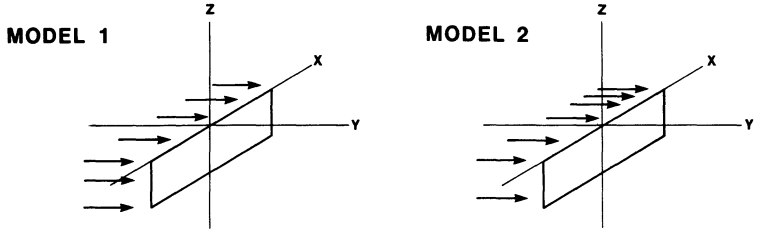

Fig. 1. Flaw interaction with uniform (Model 1) and nonuniform (Model 2) incident current densities.

Another difference in Model 2 is the introduction of the so-called Kahn effects. According to the calculations of Kahn et al.[4], the current density is depleted at the crack corners and enhanced at the crack tip. We've used results from another calculation by Spal and Kahn[5] to develop an approximate model of these effects which are incorporated in our Model 2.

The Spal and Kahn calculation provides a solution for the magnetic field in an infinite cylinder with a radial crack extending from the center of the cylinder to the surface. It is assumed that the cylinder is in a uniform magnetic field which is parallel to the cylinder axis, and that the field strength on the cylinder surface and crack surface have this constant value H_o, as indicated in Figure 2. If j_o is the current density on the surface of the cylinder in the absence of a crack, we find, by differentiating the magnetic field solution given by Spal and Kahn, that the normalized current density on the surface in the presence of a crack is given by

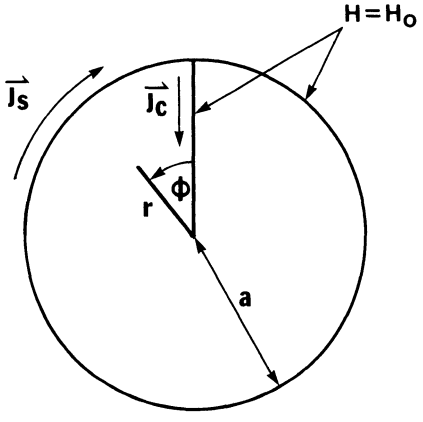

Fig. 2. Geometry for the Calculation of surface current densities.

$$j_s/j_o = \frac{J_o(ka)}{J_1(ka)} [\sin\phi \sin(ka \sin\phi)$$

$$- \sum_{n=o}^{\infty} A_n \left(\frac{2n + 1}{2ka} - \frac{j_{n+1}(ka)}{j_n(ka)}\right) \sin\left(n + \frac{1}{2}\right)\phi],$$

while the current density on the crack face is

$$j_c/j_o = \frac{J_o(ka)}{krJ_1(ka)} \sqrt{\frac{r}{a}} \sum_{n=o}^{\infty} A_n \left(n + \frac{1}{2}\right) \frac{j_n(kr)}{j_n(ka)},$$

with

$$A_n = \frac{4(1 - J_o(ka))}{(2n + 1)\pi} - \frac{8(2n + 1)}{\pi} \sum_{m=1}^{\infty} \frac{J_{2m}(ka)}{(2n + 1)^2 - 16m^2},$$

and

$$k = \frac{1 + i}{\delta}.$$

The J_n in these expressions are ordinary Bessel functions and the j_n are spherical Bessel functions.

Figures 3 and 4 are plots of the normalized current density on the cylinder surface as a function of distance from the crack, and on the crack surface as a function of depth. The dashed curve in Figure 3 is the normalized surface current as calculated from the Spal & Kahn model for $a/\delta = 2$, where a is the cylinder radius and δ is the skin depth. Calculations for other a/δ values are approximately the same, and all are fit reasonably well by the simple exponential function, $1-\exp\left((i-1)y/\delta\right)$, shown as the solid curve in Figure 3. Here we are showing only absolute values; phase variations are also fit with comparable accuracy.

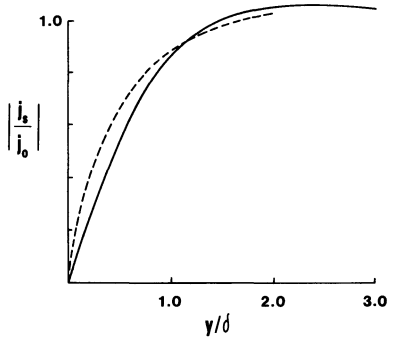

Fig. 3. Normalized current density on the surface of an infinite cylinder. The dashed curve is the exact solution; the solid curve is an approximate curve fit used in Model 2.

Figure 4 shows the normalized current density on the crack face as a function of distance from the surface divided by d, the crack depth. We note that the current vanishes at the crack corner on the surface and has a $\sqrt{\text{distance}}$ singularity at the crack tip--these are the two Kahn effects mentioned earlier. Also, we find once again that we can curve fit the data with the simple function

$$j_c/j_o = -\frac{3Ze^{-2Z/d}}{\sqrt{d^2 + Zd}}.$$

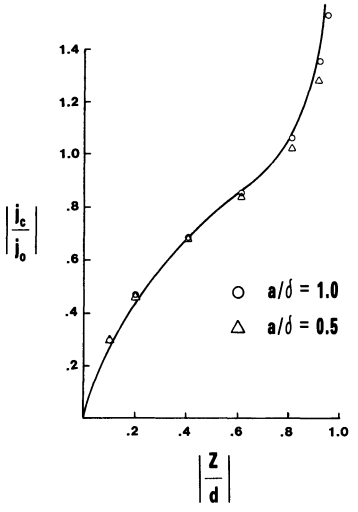

Fig. 4. Normalized current density on the crack face. Points are the exact solution; the curve is an approximation used in Model 2.

Our new flaw interaction model (Model 2) is based on the assumption that the currents on the surface of a flat test piece and along the crack face are proportional to the incident current density, which may vary with position along the crack, and have functional forms given by the two curve fits derived above. Thus, if ℓ is the length of the crack along the x axis of Figure 1 and if d is the crack depth, then the current density on the Z=0 surface is assumed to be

$$j_y(x,y) = j_y^o(x) \begin{cases} 1 - e^{-(1-i)\frac{|y|}{\delta}} & \text{for } |x| \leq \ell/2 \\ 1 & \text{for } |x| > \ell/2 \end{cases}$$

while the current density on the crack face is

$$j_z(x,z) = j_y^o(x)\ \frac{3Ze^{2Z/d}}{\sqrt{d^2 + Zd}},$$

where $j_y^o(x)$ is the component of the incident current density normal to the crack face. Substitution of these approximate current densities in the surface integral form of the reciprocity theorem leads, in the usual way[6], to an integral expression for the ECP flaw response.

Even though this is a simplified model of the current perturbation, the calculation of ECP probe response based on this model leads to a four-dimensional Fourier integral which is much too difficult to handle. For this reason we've introduced one more approximation, in this case to the incident current density $j_y^o(x)$, which allows us to do 2 of the 4 integrals analytically and therefore makes the model computationally tractable.

Figure 5 shows the induced current density, divided by its peak value, as a function of distance from the center of the induction coil, divided by the distance to the peak. The points are values obtained by numerical evaluation using a model equivalent to that of Dodd and Deeds[7] and represent frequencies of 20 kHz to 2 MHz at depths below the surface from zero to 0.05 in. The solid curve is the function

$$j(r)/jp = \frac{r}{rp} e^{-\frac{1}{2}[(r/rp)^2 - 1]}.$$

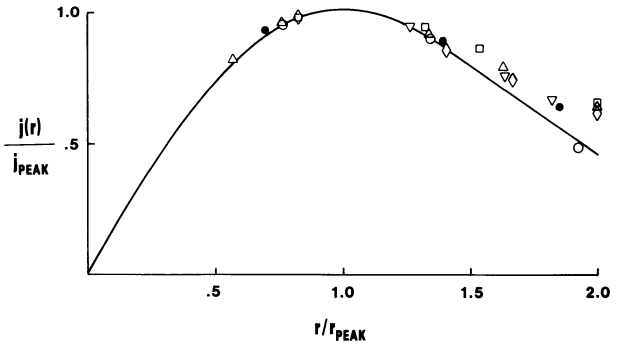

Fig. 5. Normalized incident currnt density. Points are exact calculations; the curve is an approximate fit used in Model 2.

Again we see that a curve fit to the amplitude of the induced current works fairly well. Phase calculations show that the phase is nearly constant in the vicinity of the peak and we have therefore ignored phase variation as a function of distance.

NUMERICAL RESULTS

If we calculate the real part of the signal as the probe is scanned along the length of a crack we obtain a bipolar curve with positive and negative peaks[1,2], and we may therefore use the peak-to-peak amplitude as a measure of flaw signal strength. Experimentally, of course, we

usually don't look at the real part but instead some complex component chosen so as to maximize the flaw signal. This amounts to dividing our calculated signal by the cosine of some phase angle which we've done in a few cases using the phase at the larger of the two peaks.

Plots of peak-to-peak amplitude as a function of frequency for Model 1, the uniform field model, and for Model 2 are shown in Figure 6. Both models show generally the same trend as a function of frequency but there is serious disagreement in signal amplitude, which tells us that calculated flaw signals are quite sensitive to the details of the flaw interaction model. The arrows at the low and high frequency extremes indicate what happens when we divide by the cosine of the phase, and from this we can see that the difference between the two models is mostly in phase at low frequency and in absolute value at high frequency. The changes we obtain by dividing by the cosine of the phase will, of course, have no effect on the signal-to-noise ratios because the cosines cancel when we take the ratio.

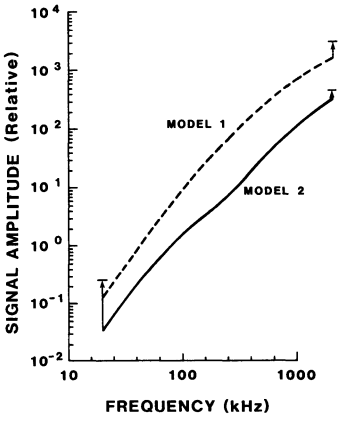

Fig. 6. Real parts of signal amplitudes from Models 1 and 2. Arrows indicate changes caused by dividing by the cosine of the phase at the signal peak.

In calculating signal-to-noise we've looked at two sources of noise. One is a change in liftoff and the other is a surface or near surface anomaly which we've modeled as small cubic void at the surface. This choice of a surface noise model is rather arbitrary--it's intended to be typical of near-surface noise sources insofar as frequency dependence is concerned and, we think, should suffice for modeling the frequency dependence of signal-to-noise.

Figure 7a gives plots of signal-to-liftoff noise for both flaw models and two flaw sizes. The trends are generally the same for both models and they tell us that higher frequencies tend to give better signal-to-noise figures. On the other hand, similar plots for signal-to-surface noise shown in Figure 7b indicate that in this case lower frequencies are favored. This agrees with our experience with the ECP probe for which liftoff noise is usually low and most of the background comes from near surface material inhomogeneities. We would expect that

lower frequencies should be better in such cases because the smaller skin depths at higher frequency should tend to enhance surface anomalies relative to sub-surface features.

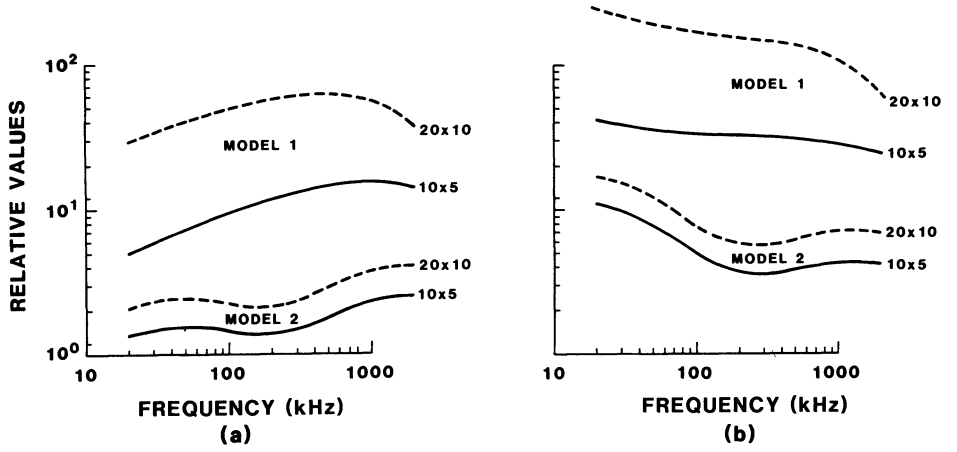

Fig. 7. Signal-to-noise ratios for (a) liftoff noise and (b) surface noise. Flaw dimensions are in units of 0.001 inch.

Finally, we've taken a brief look at phase as a function of frequency to see if there might be some hope of measuring flaw depth using phase shifts at two or more frequencies. The data plotted in Figure 8 say that there is such a possibility because the shapes of the curves show a definite depth dependence. Thus, if we measure the phase at two frequencies, the slope of the line through the two points on a phase vs. frequency plot should provide a measure of flaw depth.

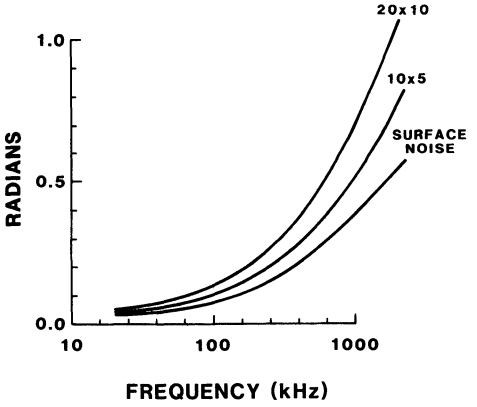

Fig. 8. Phase shift as a function of frequency and flaw depth.

In summary then, we've shown, through our calcualtions for two different flaw interaction models, that signal amplitude and phase are quite sensitive to the details of the models. In spite of this problem, signal/noise trends as a function of frequency are generally the same for both models, and they tell us that high frequencies are favored if

liftoff noise is the main problem and low frequencies are better if the principal source of noise is near surface irregularities in the material. Finally, we've looked very briefly at phase vs. frequency and flaw depth and our results suggest that multifrequency phase data may provide depth information.

ACKNOWLEDGEMENT

This work was sponsored by the Center for Advanced Nondestructive Evaluation, operated by the Ames Laboratory, USDOE, for the Air Force Wright Aeronautical Laboratories/Materials Laboratory under Contract No. W-7405-ENG-82 with Iowa State University.

REFERENCES

1. R.E. Beissner, C.M. Teller, G.L. Burkhardt, R.T. Smith and J.R. Barton, Detection and Analysis of Electric Current Perturbation Caused by Defects, in: "Eddy-Current Characterization of Materials and Structures," ASTM STP 722, G. Birnbaum and G. Free, eds., American Society for Testing and Materials, Philadelphia (1981).

2. R.E. Beissner, M.J. Sablik and C.M. Teller, Electric Current Perturbation Calculations for Half-Penny Cracks, in "Review of Progress in Quantitative Nondestructive Evaluation, Volume 2," D.O. Thompson and D.E. Chimenti, eds., Plenum, New York (1983).

3. R.E. Beissner and M.J. Sablik, Theory of Electric Current Perturbation Probe Optimization, in "Review of Progress in Quantitative Nondestructive Evaluation Volume 3," D.O. Thompson and D.E. Chimenti, eds., Plenum, New York (1984).

4. A.H. Kahn, R. Spal and A. Feldman, Eddy Current Losses due to a Surface Crack in Conducting Material, J. Appl. Phys. 48:4454 (1977).

5. R. Spal and A.H. Kahn, Eddy Currents in a Conducting Cylinder with a Crack, J. Appl. Phys. 50:6135 (1979).

6. B.A. Auld, Theoretical Characterization and Comparison of Resonant-Probe Microwave Eddy-Current Testing with Conventional Low-Frequency Eddy-Current Methods, in : "Eddy-Current Characterization of Materials and Structures," ASTM STP 722, G. Birnbaum and G. Free, eds., American Society for Testing and Materials, Philadelphia (1981).

7. C.V. Dodd and W.E. Deeds, Analytical Solutions to Eddy-Current Probe-Coil Problems, J. Appl. Phys. 39:2829 (1968).